Supplementary Information

The Influence of Molecular Conformation on the Photophysics of Organic Room Temperature Phosphorescent Luminophores

Rongjuan Huang,[1] Jonathan S. Ward,[2] Nadzeya A. Kukhta,[2] João Avó,[3] Jamie Gibson,[4] Thomas Penfold,*[4] João C. Lima,[5] Andrei S. Batsanov,[2] Mário N. Berberan-Santos,[3] Martin R. Bryce,[2] and Fernando B. Dias.*[1]

[1]Physics Department, Durham University, South Road, Durham, DH1 3LE, UK.

E-mail: f.m.b.dias@durham.ac.uk

[2]Chemistry Department, Durham University, South Road, Durham, DH1 3LE, UK.

[3]CQFM-IN and IBB-Institute for Bioengineering and Biosciences, Instituto Superior Técnico, Universidade de Lisboa, 1049-001 Lisboa, Portugal

[4]Chemistry-School of Natural and Environmental Sciences, Newcastle University, Newcastle upon Tyne, NE1 7RU, UK.

E-mail: tom.penfold@newcastle.ac.uk

[5]REQUIMTE, Departamento de Química, Faculdade de Ciências e Tecnologia, Universidade Nova de Lisboa, 2829-516 Caparica, Portugal.

S1- General chemistry experimental details

All reactions were carried out under an argon atmosphere unless otherwise stated. Starting materials were purchased commercially and were used as received. Solvents were dried using an Innovative Technology solvent purification system and were stored in ampoules under argon.

TLC analysis was carried out using Merck Silica gel 60 F_{254} TLC plates and spots were visualised using a TLC lamp emitting at 365, 312 or 254 nm. Silica gel column chromatography was performed using silica gel 60 purchased from Sigma Aldrich.

^{1}H and ^{13}C NMR spectroscopy was carried out on Bruker AV400, Varian VNMRS 500 and 700, and Varian Inova 500 NMR spectrometers. Residual solvent peaks were referenced as described in the literature[1], and all NMR data was processed in MestReNova V11.

Melting points were carried out on a Stuart SMP40 machine with a ramping rate of 4 °C min^{-1}. Videos were replayed manually to determine the melting point.

High resolution mass spectrometry was carried out on a Waters LCT Premier XE using ASAP ionisation. Samples were analysed directly as solids.

Elemental analysis was performed on an Exeter Analytical E-440 machine

1-Methylphenothiazine, 1-*iso*-propylphenothiazine and 1-*tert*-butylphenothiazine were prepared according to literature procedures.[1]

S2 – Synthetic procedures and characterisation data

Synthesis of 2,8-Bis(10*H*-phenothiazin-10-yl)dibenzo[*b,d*]thiophene (DPTZ-DBT)

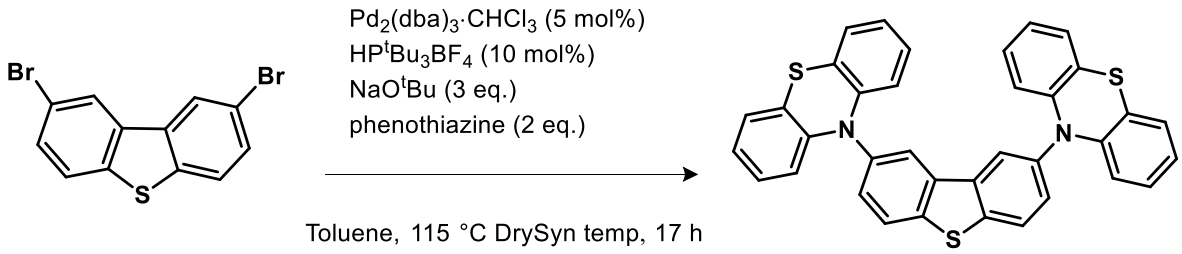

2,8-Dibromodibenzothiophene (268 mg, 0.783 mmol, 1 eq.) and phenothiazine (312 mg, 1.566 mmol, 2 eq.) were dried under vacuum for 30 min in a two-neck 100 mL round-bottomed flask fitted with a reflux condenser. The flask was back-filled with argon and dry toluene (20 mL) was added. The reaction mixture was bubbled with argon for 30 min, then $Pd_2(dba)_3{\cdot}CHCl_3$ (41 mg, 39 μmol, 0.05 eq.) and $HP^tBu_3BF_4$ (23 mg, 79 μmol, 0.10 eq.) were added and the reaction mixture was bubbled with argon for a further 30 min. NaO^tBu (225 mg, 2.34 mmol, 3 eq.) was added under a high flow of argon and the reaction was then heated to 115 °C (DrySyn kit temperature) with stirring for 17 h. At the end of the reaction $CHCl_3$ (70 mL) was added followed by water (70 mL). The organic layer was separated and the aqueous layer was extracted further with $CHCl_3$ (2 × 70 mL). The organic extracts were combined and were dried with $MgSO_4$ and filtered. The solvent was removed under reduced pressure and the crude mixture was purified by silica gel column chromatography with gradient elution from 20% *v/v* $CHCl_3$/hexane switching to 100% $CHCl_3$ in 20% increasing increments. Removal of solvent under reduced pressure gave a yellow solid. Recrystallization of the residue from boiling hexane with slow addition of chloroform followed by hot filtration and cooling to −18 °C gave

DPTZ-DBT as a cream-yellow crystalline solid (205 mg, 45% yield). The molecule was sublimed by heating at > 300 °C under vacuum (9×10^{-2} mbar). Crystals suitable for X-ray diffraction were obtained by slow evaporation from $CDCl_3$ and allowing for complete solvent evaporation.

^{1}H NMR (400 MHz, DMSO-d_6) δ 8.69 (d, *J* = 2.0 Hz, 2H), 8.40 (d, *J* = 8.4 Hz, 2H), 7.62 (dd, *J* = 8.4, 2.0 Hz, 2H), 7.07 (dd, *J* = 7.4, 1.7 Hz, 4H), 6.92 – 6.86 (m, 4H), 6.83 (td, *J* = 7.4, 1.4 Hz, 4H), 6.20 (dd, *J* = 8.1, 1.4 Hz, 4H). ^{13}C NMR (151 MHz, DMSO-d_6) δ 143.8, 139.3, 137.5, 137.4, 130.1, 127.3, 126.5, 125.7, 125.2, 122.6, 119.0, 116.0. HRMS-ASAP$^+$ m/z calculated for $C_{36}H_{23}N_2S_3$ $[M+H]^+$ 579.1023, found: 579.1018; Anal. Calc. for $C_{36}H_{22}N_2S_3$ C, 74.71; H, 3.83; N, 4.84. Found: C, 74.68; H, 3.79; N, 4.87; m.p. 304 – 306 °C.

Synthesis of 2,8-bis(1-methyl-10*H*-phenothiazin-10-yl)dibenzo[*b,d*]thiophene (DPTZ- Me-DBT)

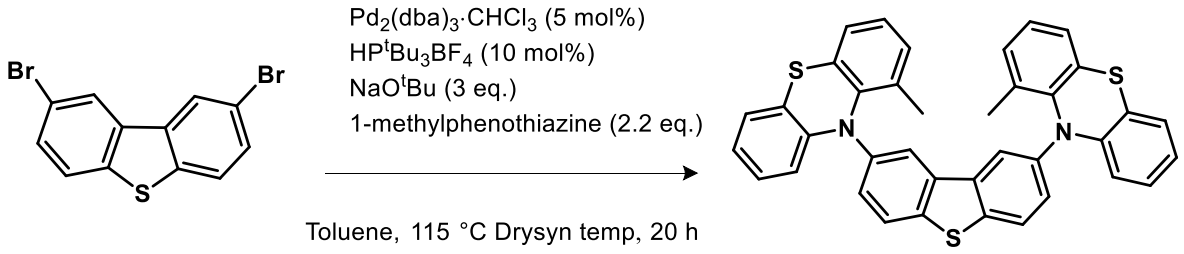

2,8-Dibromodibenzothiophene (1.09 g, 3.20 mmol, 1 eq.) and 1-methylphenothiazine (1.43 g, 7.00 mmol, 2.2 eq.) were dried under vacuum for 30 min in a two-neck round-bottomed 100 mL flask fitted with a reflux condenser. The flask was back-filled with argon and then dry toluene (30 mL) was added. The solution was bubbled with argon for 30 min, then $Pd_2(dba)_3{\cdot}CHCl_3$ (165 mg, 160 μmol, 0.05 eq.) and $HP^tBu_3BF_4$ (93 mg, 320 μmol, 0.1 eq.) were added and the reaction mixture was bubbled with argon for an additional 30 min. NaO^tBu (0.92 g, 9.57 mmol, 3 eq.) was added under a high flow of argon and the reaction was heated to 115 °C (DrySyn kit temperature) with stirring for 20 h. After being cooled down to room temperature, the reaction mixture was quenched with water (50 mL) and extracted with $CHCl_3$ (2 × 70 mL). The combined organic layers were dried with $MgSO_4$ and filtered. The solvent was removed under reduced pressure and the crude mixture was purified by silica gel chromatography with gradient elution from 25% *v/v* $CHCl_3$/hexane switching to 100% $CHCl_3$ in 25% increasing increments. Removal of solvent under reduced pressure resulted in product as a yellow solid. Recrystallization from 20% *v/v* $CHCl_3$/hexane mixture gave **DPTZ–Me-DBT** as a greenish solid (1.34 g, 69% yield). Crystals suitable for X-ray diffraction were obtained by slow evaporation from $CHCl_3$/hexane (30/70 *v/v*).

^{1}H NMR (700 MHz, CD_2Cl_2): δ 7.63 (d, *J* = 7.8 Hz, 2H), 7.52 (d, *J* = 7.8 Hz, 2H), 7.49 (d, *J* = 7.5 Hz, 2H), 7.43 (t, *J* = 7.7 Hz, 2H), 7.38 (d, *J* = 7.4 Hz, 2H), 7.32 (t, *J* = 8.3 Hz, 2H), 7.29 (d, *J* = 7.6 Hz, 2H), 7.24 (t, *J* = 7.6 Hz, 2H), 6.99 (d, *J* = 2.5 Hz, 2H), 6.77 (dd, *J* = 8.8, 2.6 Hz, 2H), 2.37 (s, 6H); ^{13}C NMR (176 MHz, CD_2Cl_2): δ 143.9, 142.8, 141.0, 137.9, 137.1, 136.7, 136.4, 131.9, 130.1, 129.5, 129.2, 127.4, 126.9, 126.8, 126.8, 123.3, 114.7, 106.0, 18.1.; HRMS-ASAP+ m/z calculated for $C_{38}H_{26}N_2S_3$ [M]+ 606.1258, found: 606.1260; Anal. Calc. for $C_{38}H_{26}N_2S_3$ C, 75.21; H, 4.32; N, 4.62. Found: C, 74.89; H, 4.69; N, 4.22; m.p. 235 – 237 °C.

Synthesis of 2,8-bis(1-*iso*propyl-10*H*-phenothiazin-10-yl)dibenzo[*b,d*]thiophene (DPTZ-^{i}Pr-DBT)

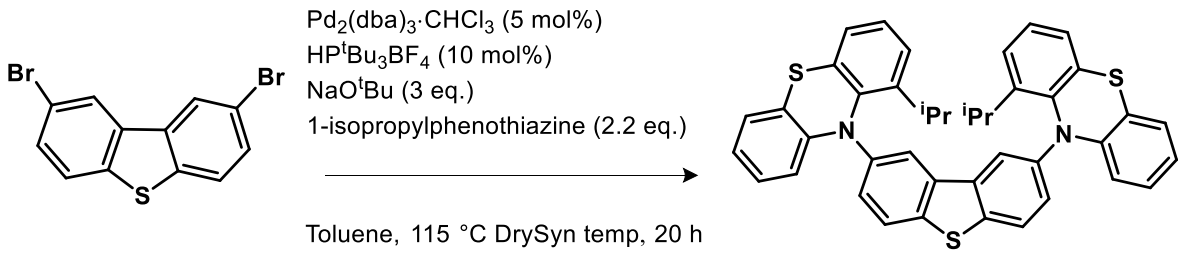

DPTZ–^{i}Pr-DBT was prepared using the procedure for **DPTZ-Me-DBT**; 2,8-dibromodibenzothiophene (400 mg, 1.17 mmol, 1 eq.), 1-*iso*-propylphenothiazine (620 mg, 2.56 mmol, 2.2 eq.), $Pd_2(dba)_3{\cdot}CHCl_3$ (66 mg, 63 μmol, 0.05 eq.), $HP^tBu_3BF_4$ (34 mg, 117 μmol, 0.1 eq.), NaO^tBu (337 mg, 3.5 mmol, 3 eq.) and toluene (25 mL) were heated to 115 °C (DrySyn kit temperature) with stirring for 20 h. After extraction with $CHCl_3$ as detailed previously, the crude mixture was purified by silica gel column chromatography eluting with 20% *v/v* $CHCl_3$/hexane. Removal of solvent under reduced pressure and recrystallization from a 20% *v/v* $CHCl_3$/hexane mixture gave **DPTZ-^{i}Pr-DBT** as a white solid (456 mg, 59% yield). Crystals suitable for X-ray diffraction were obtained by slow evaporation from $CHCl_3$/hexane (30/70 *v/v*).

^{1}H NMR (700 MHz, CD_2Cl_2) δ 7.61 (dd, *J* = 7.9, 1.4 Hz, 2H), 7.54 (dd, *J* = 7.8, 1.4 Hz, 2H), 7.42 – 7.46 (m, 4H), 7.37 – 7.40 (m, 4H), 7.36 (d, *J* = 7.5 Hz, 2H), 7.33 (td, *J* = 7.6, 1.3 Hz, 2H), 7.33 (d, *J* = 7.0 Hz, 2H), 6.87 (d, *J* = 2.1 Hz, 2H), 6.73 (dd, *J* = 8.8, 2.5 Hz, 2H), 3.45 (hept, *J* = 6.8 Hz, 2H), 1.15 (d, 12H, *J* = 6.8 Hz); ^{13}C NMR (176 MHz, CD_2Cl_2): δ 148.7, 144.9, 143.0, 139.6, 137.7, 136.9, 136.3, 131.8, 130.1, 129.2, 127.7, 127.4, 127.0, 126.8, 125.1, 123.1, 114.6, 105.9, 29.0; HRMS-ASAP+ m/z calculated for $C_{42}H_{34}N_2S_3$ [M]+ 662.1884, found:662.1880; Anal. Calc. for $C_{42}H_{34}N_2S_3$ C, 76.10; H, 5.17; N, 4.23. Found: C, 75.80; H, 5.16; N, 4.16; m.p. 287 – 289 °C.

Synthesis of 2,8-Bis(1-tertbutyl-phenothiazin-10-yl)dibenzo[*b,d*]thiophene (DPTZ-^{t}Bu-DBT)

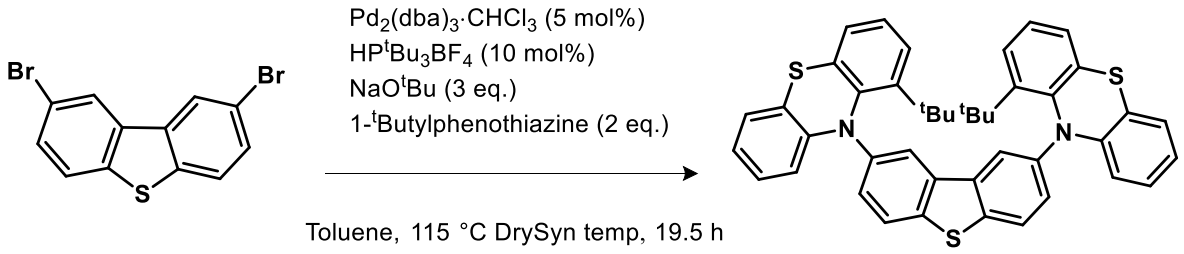

2,8-Dibromodibenzothiophene (153 mg, 0.446 mmol, 1 eq.) and 1-^{t}butylphenothiazine (228 mg, 0.892 mmol, 2 eq.) were dried under vacuum for 30 min in a two-neck 100 mL round-bottomed flask fitted with a reflux condenser. The flask was back-filled with argon and dry toluene (15 mL) was added. The reaction mixture was bubbled with argon for 30 min, then $Pd_2(dba)_3{\cdot}CHCl_3$(23 mg, 22 μmol, 0.05 eq.) and $HP^tBu_3BF_4$ (13 mg, 45 μmol, 0.10 eq.) was added and the reaction mixture was bubbled with argon for a further 30 min. NaO^tBu (129 mg, 1.34 mmol, 3 eq.) was added under a high flow of argon and the reaction was then heated to 115 °C (DrySyn kit temperature) with stirring for 19.5 h. At the end of the reaction the solvent was removed under reduced pressure and the crude

mixture was purified by silica gel column chromatography with gradient elution from 15% *v/v* CH_2Cl_2/hexane switching to 35% CH_2Cl_2 in 10% increasing increments. Removal of solvent under reduced pressure gave product as a white solid (105 mg, 34%). The solid was sublimed by heating at > 350 °C under vacuum (9 × 10^{-2} mbar). Note: **DPTZ-^{t}Bu-DBT** was isolated a mixture of diastereomers due to restricted rotation around the donor–acceptor bonds.

^{1}H NMR (500 MHz, DMSO-d_6, 373 K) δ 7.77 (dd, *J* = 7.9, 1.3 Hz, 1H), 7.74 (dd, *J* = 7.9, 1.3 Hz, 1H), 7.65 – 7.39 (m, 14H), 6.58 – 6.50 (m, 2H), 6.41 (apr. t, *J* = 3.0 Hz, 2H), 1.42 (apr. d, *J* = 8.1 Hz, 18H), ^{13}C NMR (176 MHz, DMSO-d_6, 298 K) δ 149.3, 149.1, 146.3, 143.3, 143.2, 139.4, 139.3, 137.4, 136.1, 134.4, 134.4, 130.6, 130.6, 129.9, 129.7, 128.8, 128.6, 128.5, 127.7, 127.6, 127.3, 127.2, 127.2, 127.1, 127.0, 126.8, 122.8, 122.8, 115.5, 106.6, 35.93, 35.86, 31.42, 31.37; HRMS-ASAP$^+$ m/z calculated for $C_{44}H_{38}N_2S_3$ $[M]^+$ 690.2197, found: 690.2186; Anal. Calc. for $C_{44}H_{38}N_2S_3$: C: 76.48 H: 5.54 N: 4.05. Found: C:76.31 H: 5.48 N: 3.92; m.p. 336 – 338 °C.

S3 – ^{1}H and ^{13}C NMR spectra

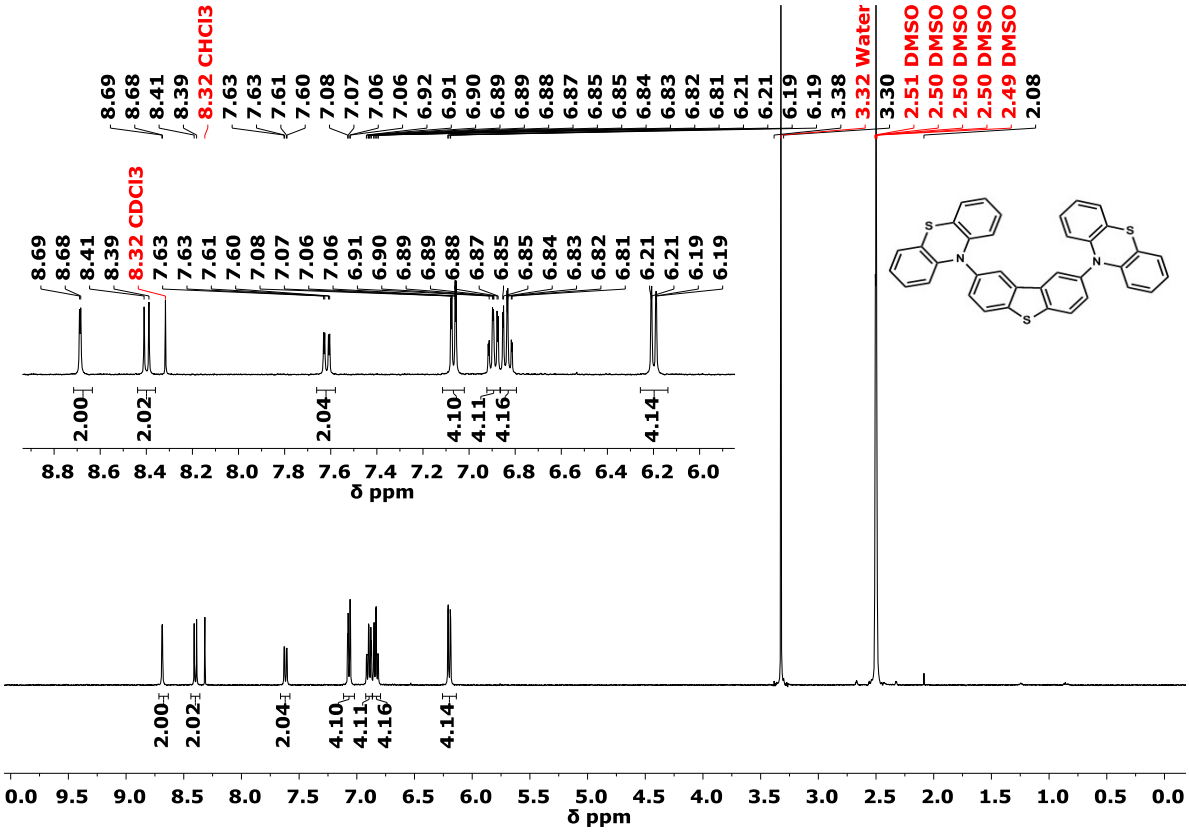

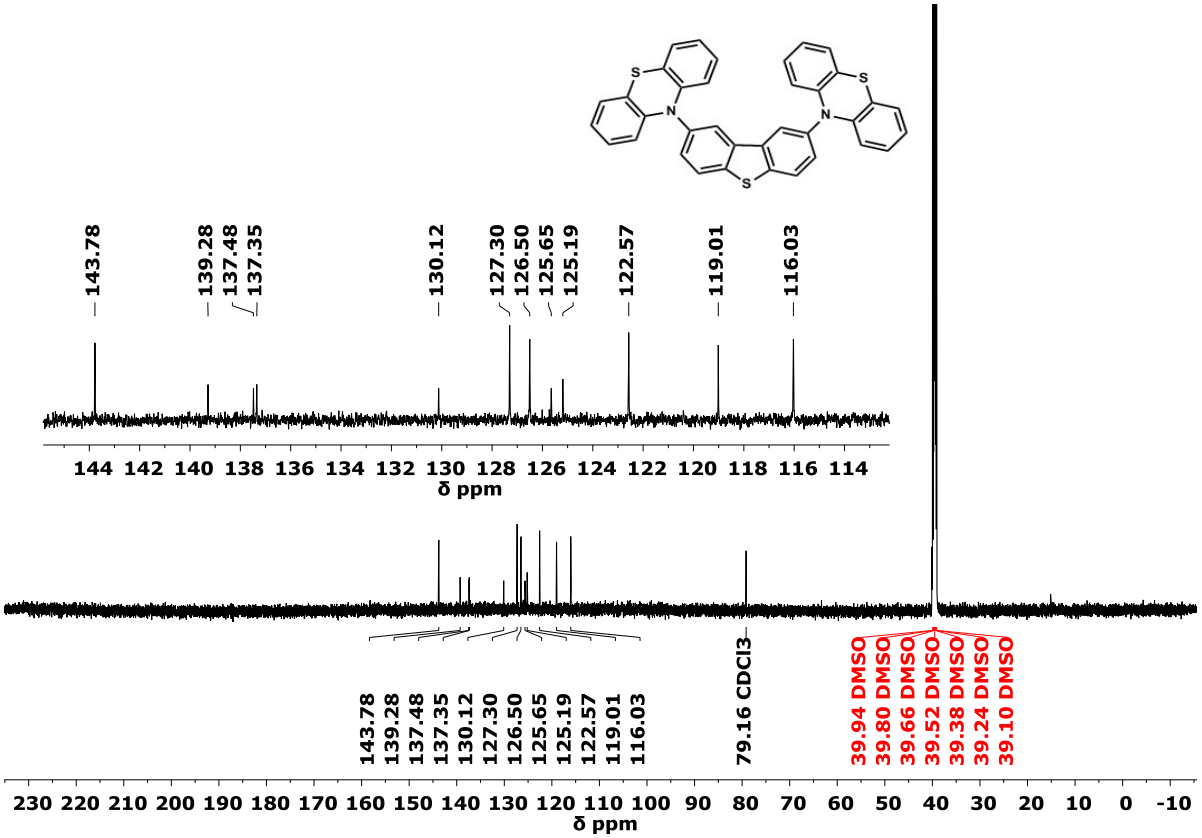
143.78
139.28
137.48
137.35
130.12
127.30
126.50
125.65
125.19
122.57
119.01
116.03
144 142 140 138 136 134 132 130 128 126 124 122 120 118 116 114
δ ppm
79.16 CDCl3
39.94 DMSO
39.80 DMSO
39.66 DMSO
39.52 DMSO
39.38 DMSO
39.24 DMSO
39.10 DMSO
230 220 210 200 190 180 170 160 150 140 130 120 110 100 90 80 70 60 50 40 30 20 10 0 -10
δ ppm

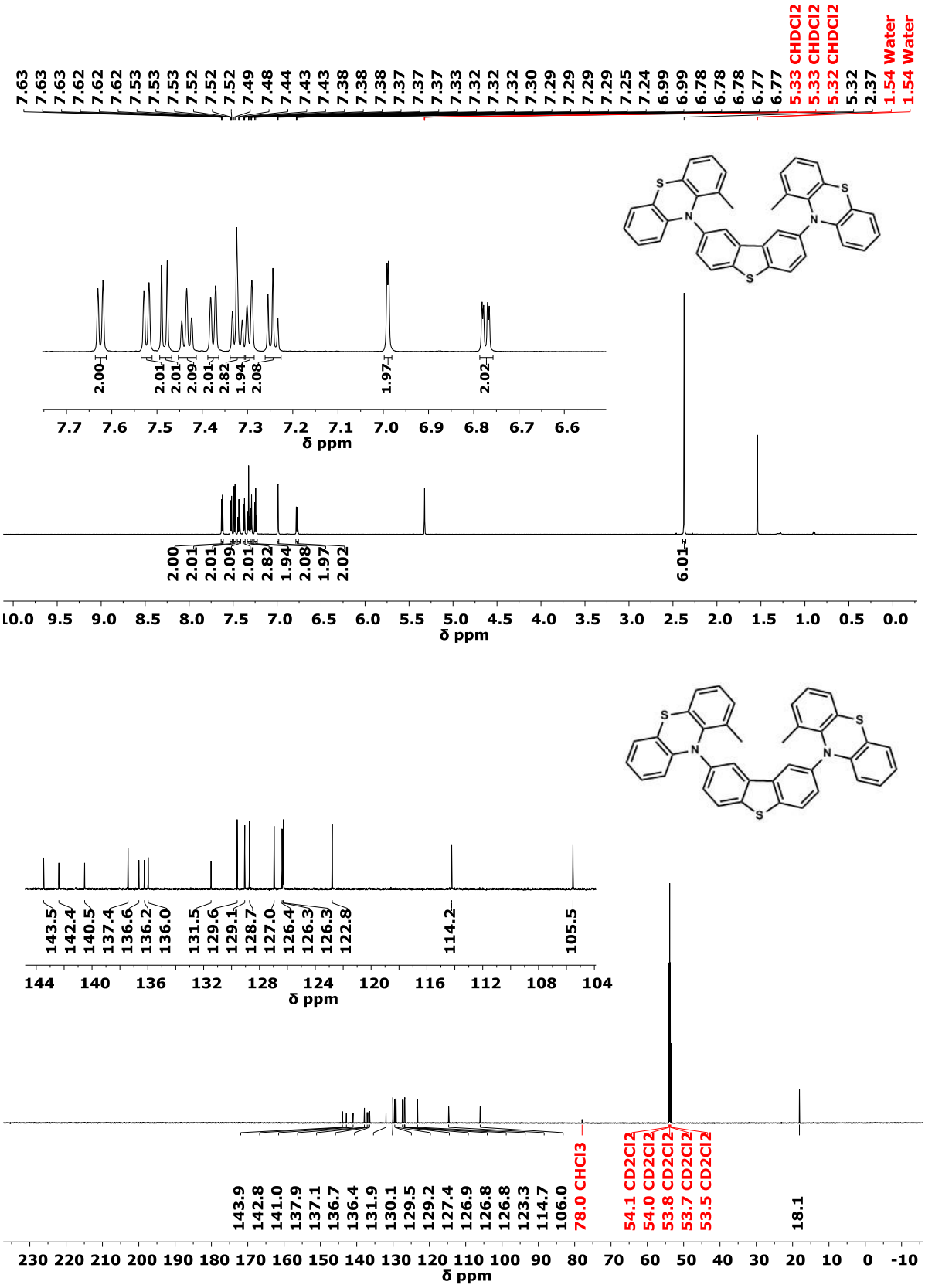
7.63 7.63 7.63 7.62 7.62 7.62 7.53 7.53 7.53 7.52 7.52 7.52 7.49 7.48 7.44 7.43 7.43 7.38 7.38 7.38 7.37 7.37 7.37 7.33 7.32 7.32 7.32 7.30 7.29 7.29 7.29 7.29 7.25 7.24 6.99 6.99 6.78 6.78 6.78 6.77 6.77 5.33 CHDCl2 5.33 CHDCl2 5.32 CHDCl2 5.32 2.37 1.54 Water 1.54 Water
2.00 2.01 2.01 2.09 2.01 2.82 1.94 2.08 1.97 2.02
7.7 7.6 7.5 7.4 7.3 7.2 7.1 7.0 6.9 6.8 6.7 6.6
δ ppm
2.00 2.01 2.01 2.09 2.01 2.82 1.94 2.08 1.97 2.02 6.01
10.0 9.5 9.0 8.5 8.0 7.5 7.0 6.5 6.0 5.5 5.0 4.5 4.0 3.5 3.0 2.5 2.0 1.5 1.0 0.5 0.0
δ ppm
S
N
S
N
S

143.5 142.4 140.5 137.4 136.6 136.2 136.0 131.5 129.6 129.1 128.7 127.0 126.4 126.3 126.3 122.8 114.2 105.5
144 140 136 132 128 124 120 116 112 108 104
δ ppm
143.9 142.8 141.0 137.9 137.1 136.7 136.4 131.9 130.1 129.5 129.2 127.4 126.9 126.8 126.8 123.3 114.7 106.0 78.0 CHCl3 54.1 CD2Cl2 54.0 CD2Cl2 53.8 CD2Cl2 53.7 CD2Cl2 53.5 CD2Cl2 18.1
230 220 210 200 190 180 170 160 150 140 130 120 110 100 90 80 70 60 50 40 30 20 10 0 -10
δ ppm
S
N
S
N
S

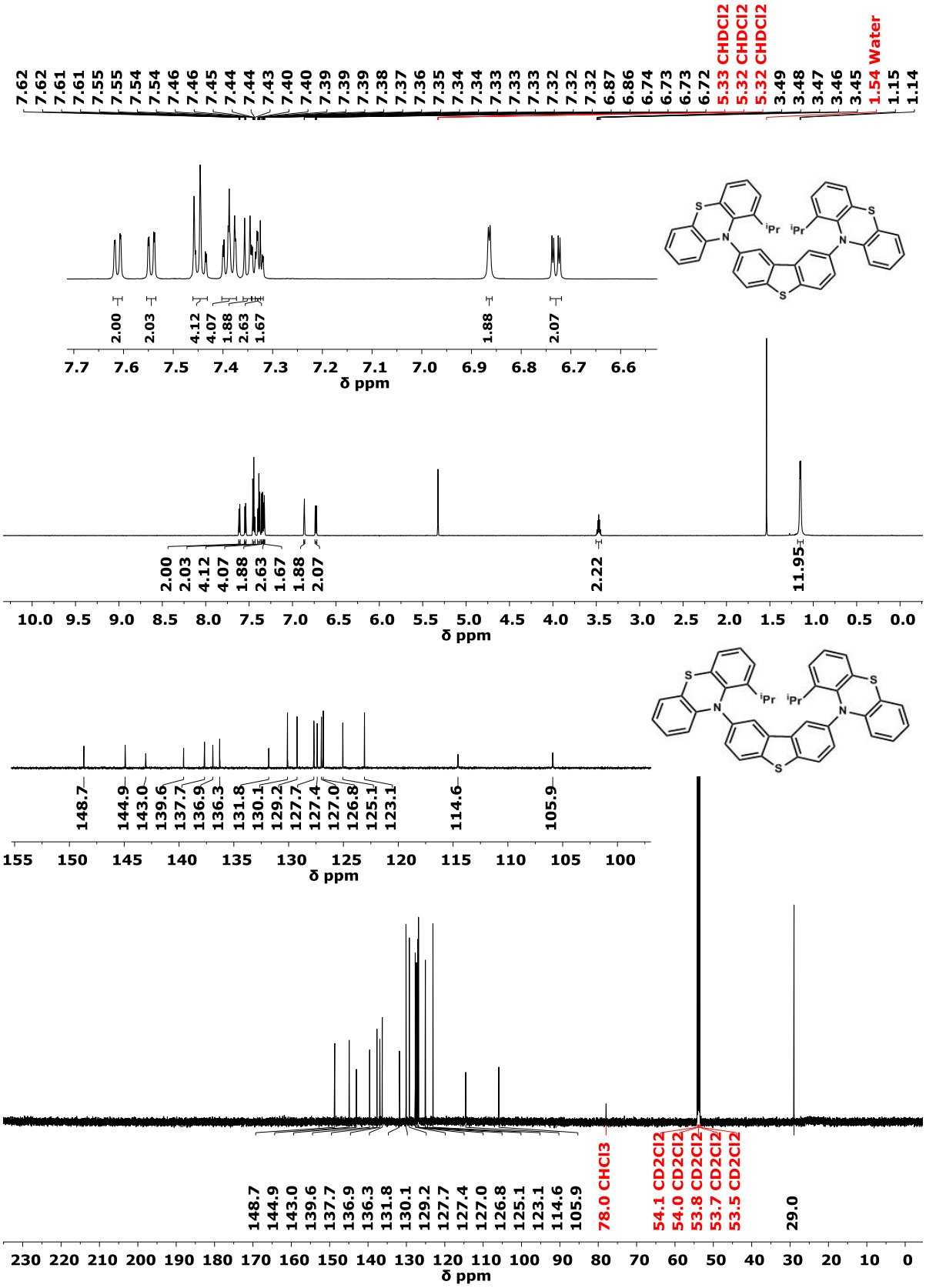
7.62 7.62 7.61 7.61 7.55 7.55 7.54 7.54 7.46 7.46 7.45 7.44 7.44 7.43 7.40 7.40 7.39 7.39 7.39 7.38 7.37 7.36 7.35 7.34 7.34 7.33 7.33 7.33 7.32 7.32 7.32 6.87 6.86 6.74 6.73 6.73 6.72 5.33 CHDCl2 5.32 CHDCl2 5.32 CHDCl2 3.49 3.48 3.47 3.46 3.45 1.54 Water 1.15 1.14
2.00 2.03 4.12 4.07 1.88 2.63 1.67 1.88 2.07
7.7 7.6 7.5 7.4 7.3 7.2 7.1 7.0 6.9 6.8 6.7 6.6
δ ppm
S N S iPr iPr
2.00 2.03 4.12 4.07 1.88 2.63 1.67 1.88 2.07 2.22 11.95
10.0 9.5 9.0 8.5 8.0 7.5 7.0 6.5 6.0 5.5 5.0 4.5 4.0 3.5 3.0 2.5 2.0 1.5 1.0 0.5 0.0
δ ppm
148.7 144.9 143.0 139.6 137.7 136.9 136.3 131.8 130.1 129.2 127.7 127.4 127.0 126.8 125.1 123.1 114.6 105.9
155 150 145 140 135 130 125 120 115 110 105 100
δ ppm
148.7 144.9 143.0 139.6 137.7 136.9 136.3 131.8 130.1 129.2 127.7 127.4 127.0 126.8 125.1 123.1 114.6 105.9 78.0 CHCl3 54.1 CD2Cl2 54.0 CD2Cl2 53.8 CD2Cl2 53.7 CD2Cl2 53.5 CD2Cl2 29.0
230 220 210 200 190 180 170 160 150 140 130 120 110 100 90 80 70 60 50 40 30 20 10 0
δ ppm

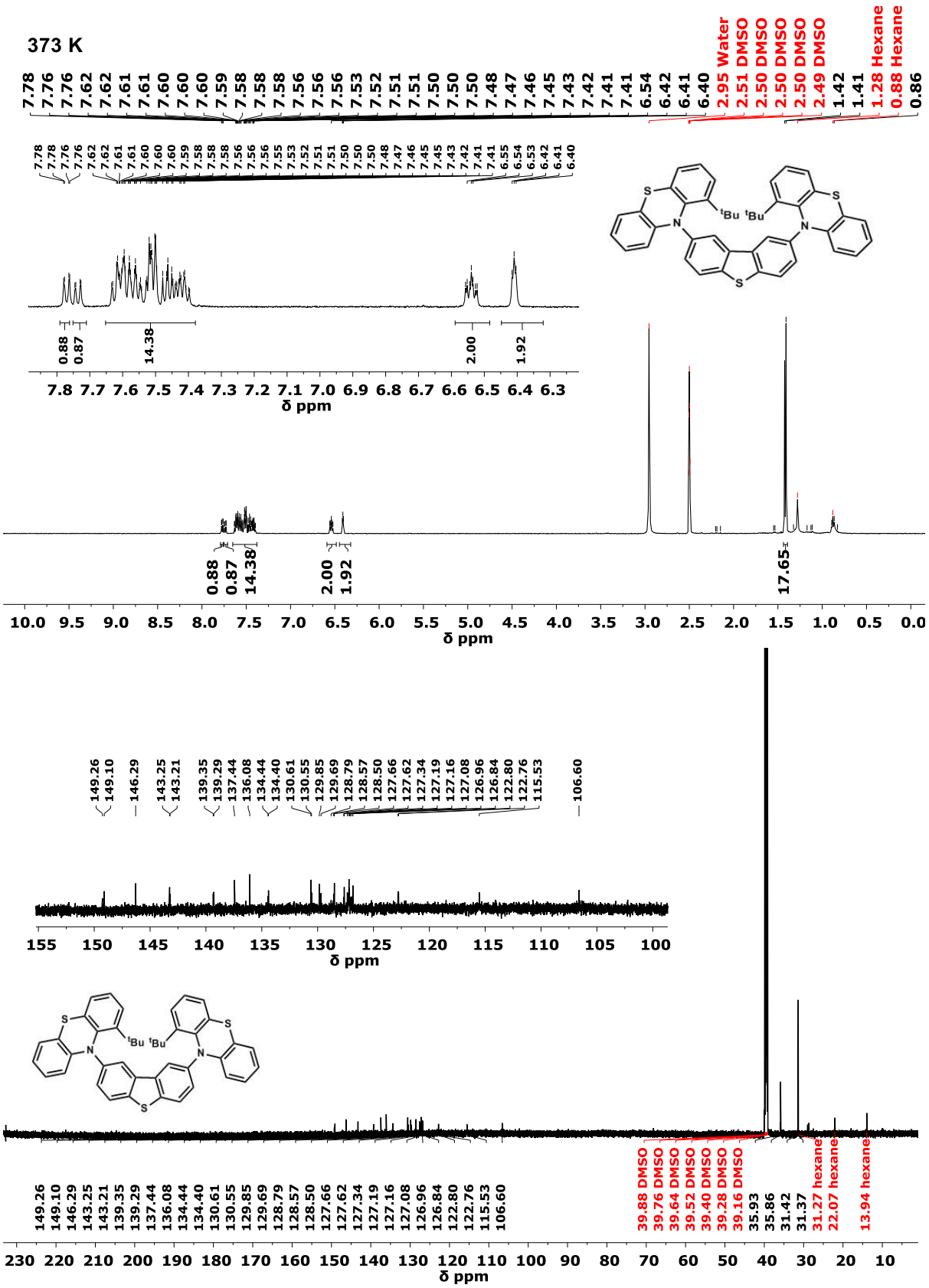
373 K
7.78 7.76 7.76 7.62 7.62 7.61 7.61 7.60 7.60 7.60 7.59 7.58 7.58 7.58 7.56 7.56 7.56 7.53 7.52 7.51 7.51 7.50 7.50 7.50 7.48 7.47 7.46 7.45 7.43 7.42 7.41 7.41 6.54 6.42 6.41 6.40
2.95 Water
2.51 DMSO
2.50 DMSO
2.50 DMSO
2.49 DMSO
1.42
1.41
1.28 Hexane
0.88 Hexane
0.86
0.88 0.87 14.38 2.00 1.92 17.65
δ ppm
149.26 149.10 146.29 143.25 143.21 139.35 139.29 137.44 136.08 134.44 134.40 130.61 130.55 129.85 129.69 128.79 128.57 128.50 127.66 127.62 127.34 127.19 127.16 127.08 126.96 126.84 122.80 122.76 115.53 106.60
39.88 DMSO
39.76 DMSO
39.64 DMSO
39.52 DMSO
39.40 DMSO
39.28 DMSO
39.16 DMSO
35.93
35.86
31.42
31.37
31.27 hexane
22.07 hexane
13.94 hexane
δ ppm

Variable temperature ^{1}H NMR spectra in DMSO-d_6 for **DPTZ-*^{i}Pr*-DBT** and **DPTZ-*^{t}Bu*-DBT**. **DPTZ-*^{t}Bu*-DBT** shows more dynamic behaviour than **DPTZ-*^{i}Pr*-DBT** with peaks sharpening at higher temperatures, suggesting a higher barrier between conformers in **DPTZ-*^{t}Bu*-DBT**. In **DPTZ-*^{i}Pr*-DBT** there is little change on increasing temperature suggesting a lower barrier to donor-acceptor bond rotation.

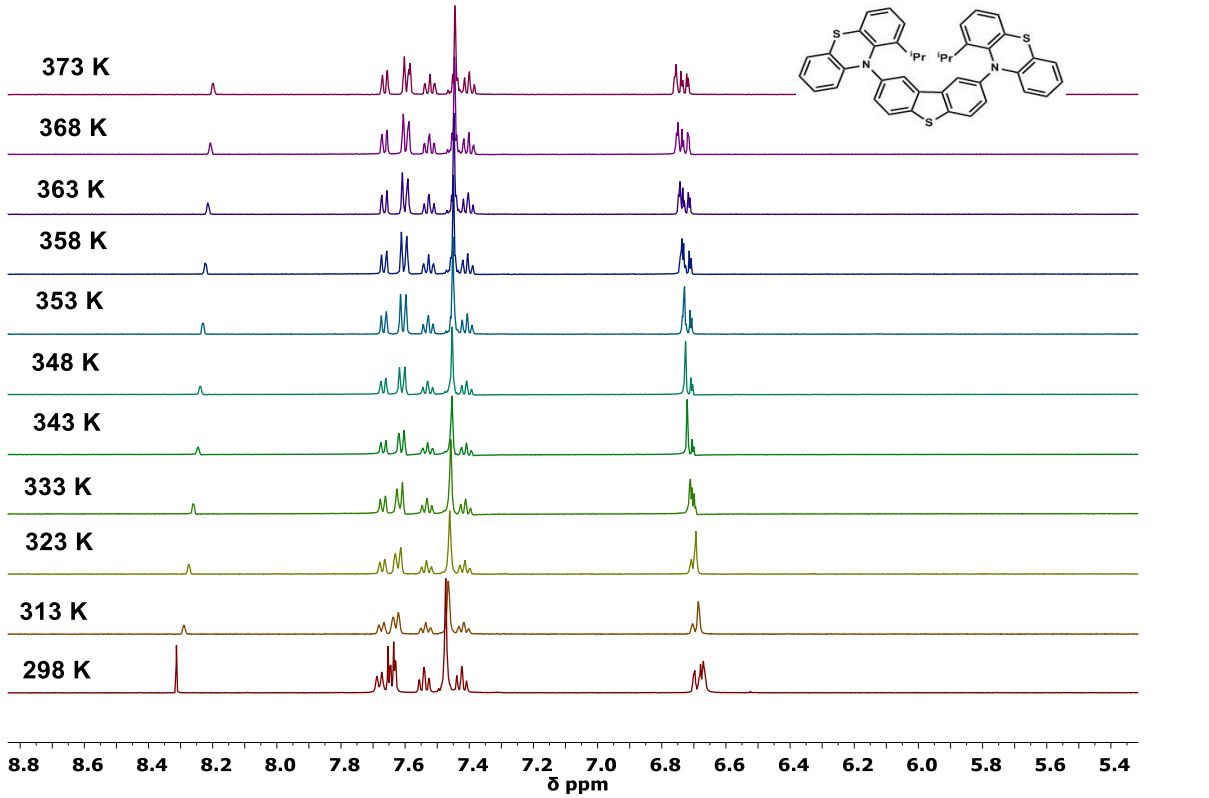

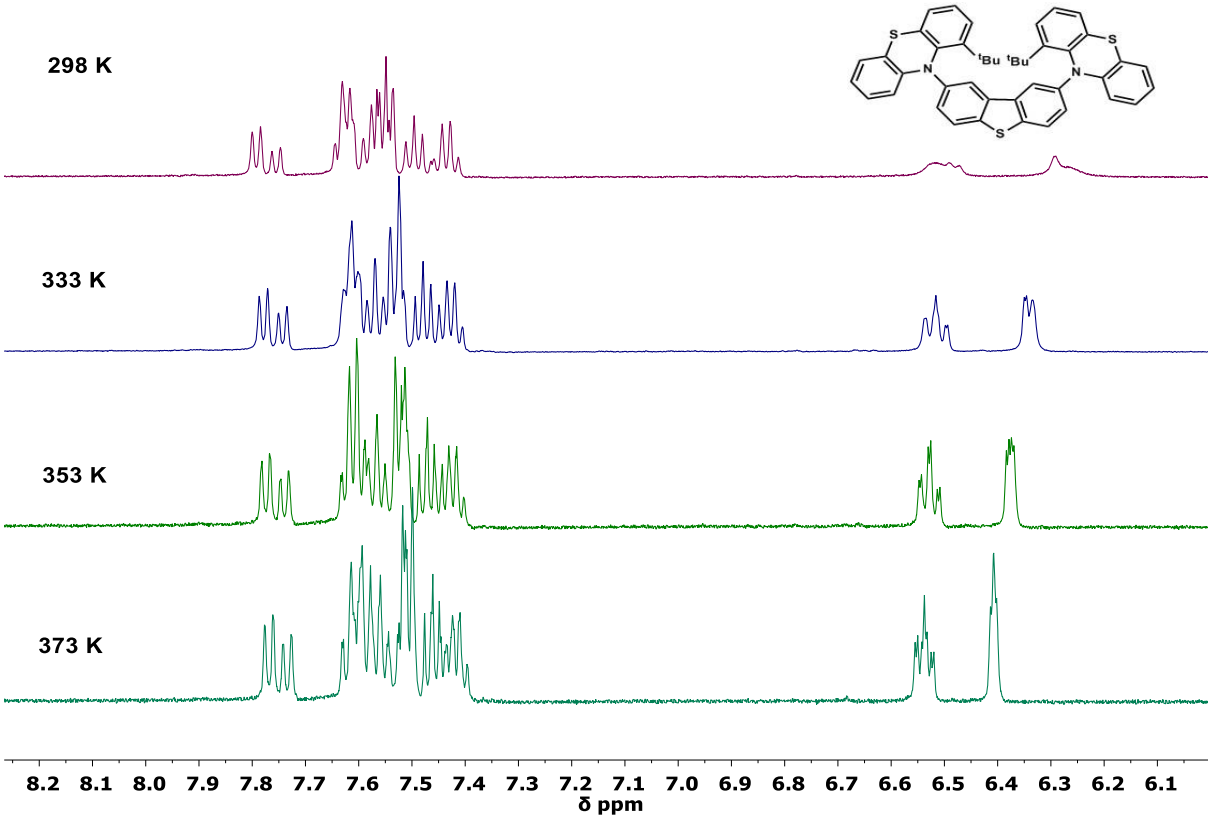

S4 – Photophysical data.

Optical spectroscopy. Absorption and emission spectra were collected using a Shimadzu UV-3600 double beam spectrophotometer, and a Jobin Yvon Fluorolog fluorescence spectrometer, respectively. Emission is independent of excitation wavelength. Steady-state fluorescence was collected with excitation at 355 nm. The luminescence temperature-dependence measurements were acquired using a model liquid nitrogen cryostat (Janis Research). Fluorescence decays under 10 ns were measured in a TCSPC system equipped with a Becker&Hickl card. The excitation source was the third harmonic (290 nm) of a ps pulsed Ti:Sa laser, Coherent, with 2 ps pulse width, and detection made using a Hamamatsu MCPT detector. The IRF of the system is under 23 ps. For longer lifetimes, a DeltaFlex TCSPC system from Horiba was used with LED excitation at 357 nm, and 1.5 ns IRF. Phosphorescence time-resolved spectra and decays were recorded using nanosecond gated luminescence, and lifetime measurements (from 1 ns to 1 s) using a pulsed Nd:YAG laser, with second harmonic emission at 355 nm (EKSPLA). Emission was focused onto a spectrograph and detected on a sensitive gated iCCD camera (Stanford Computer Optics) with sub-nanosecond resolution. Solutions were prepared with concentrations in the 10^{-5}–10^{-4} M range in different solvents, and samples were degassed using 5 freeze/thaw cycles. Films for optical characterization were prepared in zeonex matrix by drop-casting or spin-coating onto a quartz substrate with an emitter/zeonex ratio of 1: 20 (*w/w*).

For PLQY determination, films were prepared by drop-casting onto a quartz substrate with a lower emitter/zeonex ratio of 0.1: 99.9 (*w/w*) to prevent aggregation and reabsorption phenomena. Phosphorescence quantum yields were calculated using each compound ϕ_F as internal reference and the ratio of integrated areas of luminescence spectra acquired with and without oxygen, as given by equation S1,

$$\Phi_P = \Phi_F \left(\frac{I_{vac}}{I_{air}} - 1\right) \qquad \text{(S1)},$$

where I_{vac} and I_{air} are the integrals calculated for spectra in wavelength form.

Flash Photolysis Studies. Triplet lifetimes were determined in degassed benzene using a flash photolysis setup composed of a LKS. 60 ns laser photolysis spectrometer from Applied Photophysics, with a Brilliant Q-Switch Nd:YAG laser from Quantel, using the third harmonics (λ_{ex} = 355 nm, laser pulse half-width equal to 6 ns). First-order kinetics were observed for the decay of the lowest triplet state (T–T annihilation was prevented by the low excitation energy and/or low optical density at excitation wavelength, $A_{355nm} \leq 0.1$).

The transient spectra were obtained with the same apparatus by monitoring the optical density change at intervals of 10 nm over the 300–600 nm range and averaging at least 32 decays at each wavelength.

The Φ_T values for compounds **DPTZ–DBT**, **DPTZ–*Me*–DBT**, **DPTZ–^{i}*Pr*–DBT** were determined with the flash photolysis setup using the energy transfer method previously described, where 2-acetylnaphthalene and β-carotene where used as triplet standard and quencher, respectively.[2]

Compound **DPTZ-^{t}*Bu*-DBT** exhibited significant degradation under laser excitation and triplet transient absorption decays could not be separated from the photoproduct formation. Thus, a different method using a lower intensity excitation source was required. We employed a modified olefin isomerization method developed by Lamola and Hammond.[3] *Trans-β*-methylstyrene was selected as the sensitized olefin (λ_{Abs}=250 nm), which undergoes *trans* to *cis* isomerization through the sensitized triplet state, with consequent reduction of absorbance at 250 nm. A solution of **DPTZ-^{t}*Bu*-DBT** 1×10^{-5} M and *trans-β*-methylstyrene 8.5×10^{-5} M in degassed cyclohexane was irradiated while stirring for 15 min. The irradiation setup was composed of a 150 W Xenon lamp coupled with a ThorLabs 335 nm cut-off filter. The variation of the absorbance at 250 nm was followed with a Varian Cary UV-Vis spectrophotometer. The same experiment was repeated for **DPTZ-DBT** (Figure S1). Φ_T value was calculated with equation (S1).

$$\Phi_{T_A} = \frac{\Delta A_{250nm_A}}{\Delta t_A} * \frac{\Delta t_B}{\Delta A_{250nm_B}} * \Phi_{T_B} * \frac{\Phi_{ET_B}}{\Phi_{ET_A}} \qquad \text{(S2)}$$

Triplet formation quantum yield for **DPTZ-DBT** (Φ_{T_B}) was previously determined with laser-flash photolysis. Energy transfer efficiency (Φ_{ET}) was determined from triplet transient absorption decay time with (τ) and without (τ_0) olefin (equation S3).

$$\Phi_{ET} = \frac{\tau_0 - \tau}{\tau_0} \qquad \text{(S3)}$$

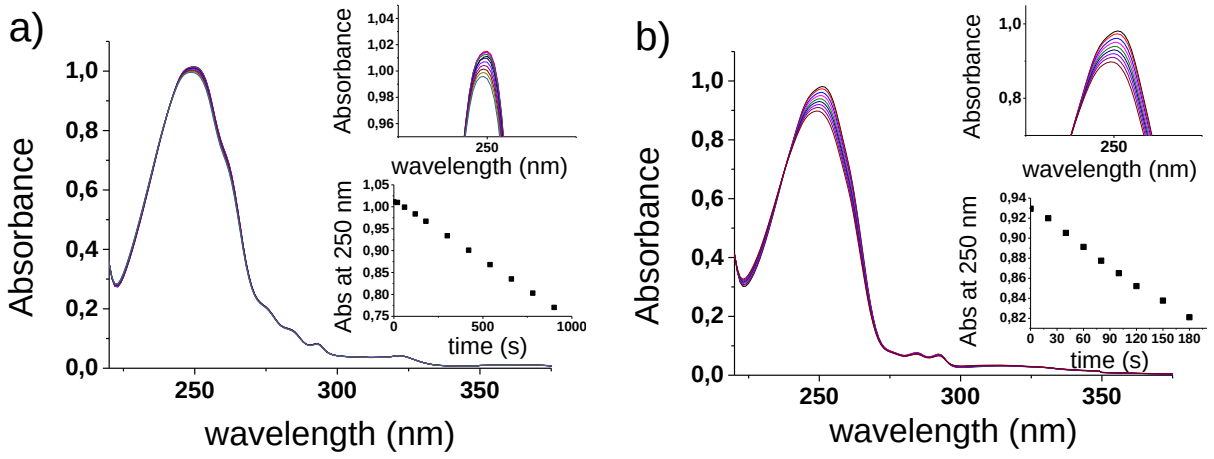

Figure S1 – Spectral variations upon irradiation of a cyclohexane solution of 8.5×10^{-5} M *trans-β*-methylstyrene and 1.0×10^{-5} M of a) **DPTZ-^{t}*Bu*-DBT** and b) **DPTZ-DBT**

UV-Vis Absorption and Fluorescence Studies.

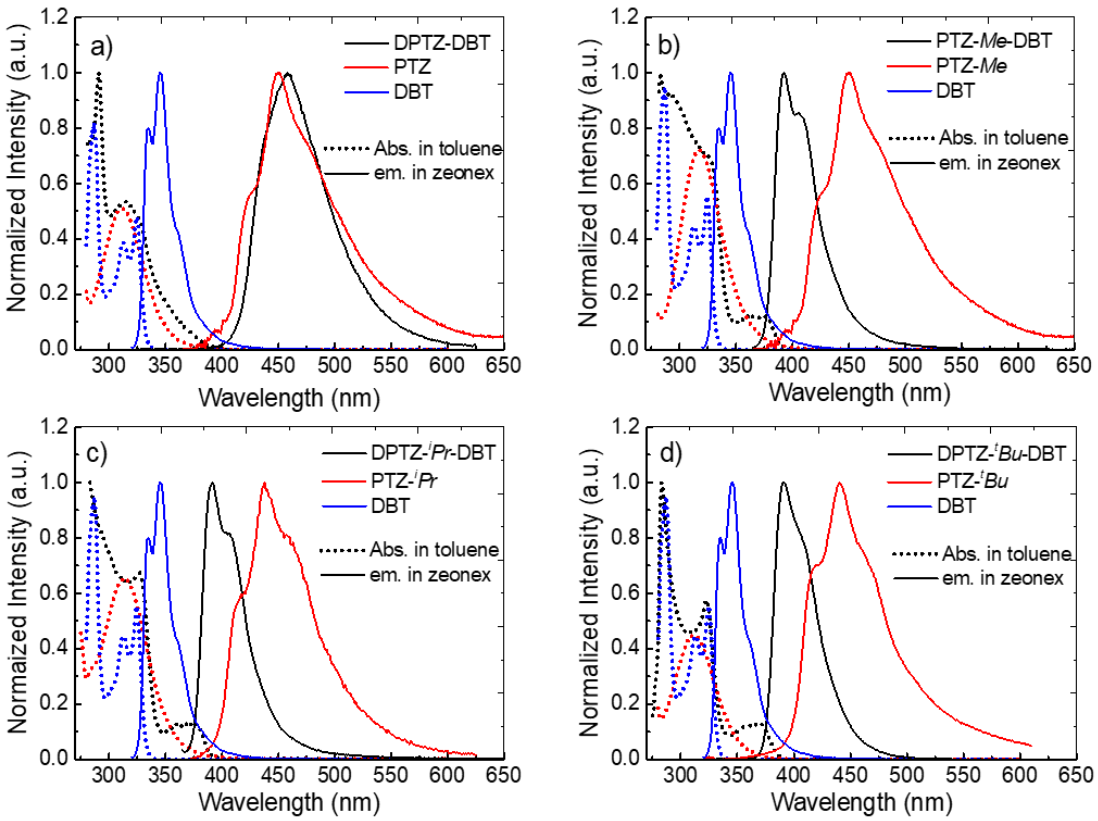

Figure S2 – Comparison of the absorption and fluorescence spectra of the parent molecule, a**) DPTZ-DBT**, and the three substituted derivatives b) **DPTZ-*Me*-DBT**, c) **DPTZ-^{i}*Pr*-DBT**, and d) **DPTZ-^{t}*Bu*-DBT** with the absorption and emission of the single units PTZ and DBT.

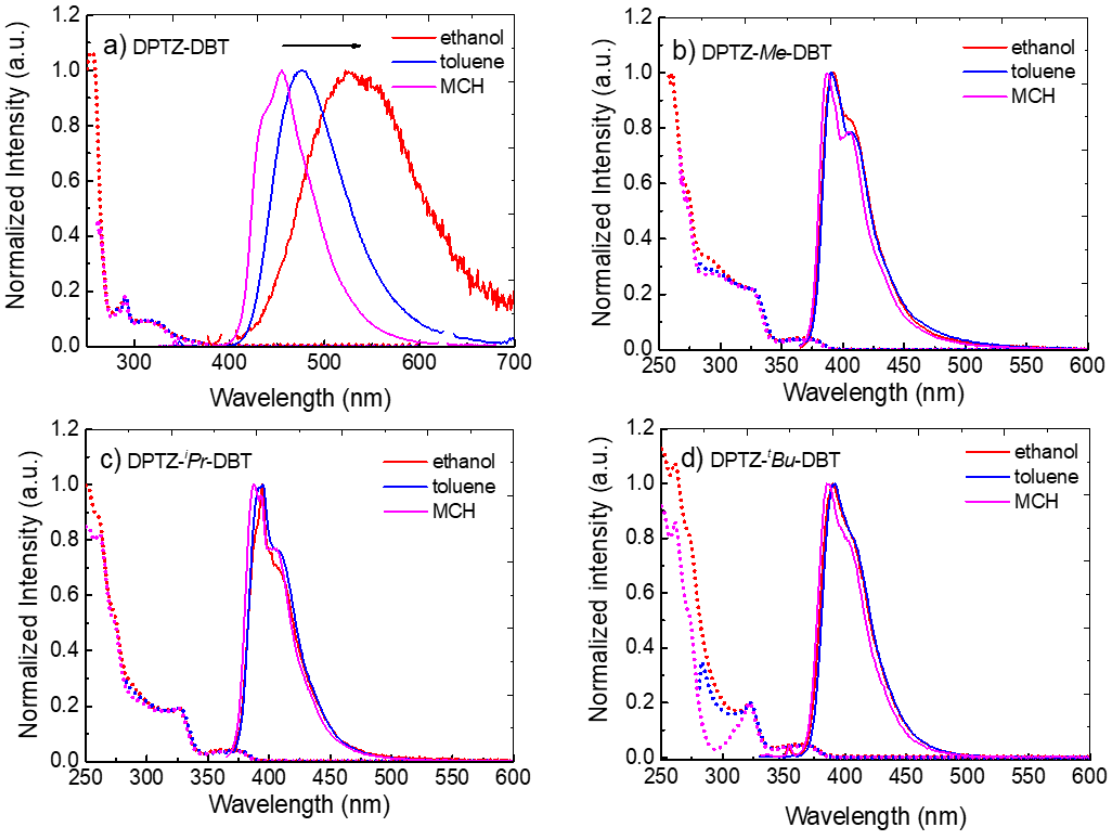

Figure S3 – Comparison of the absorption and fluorescence spectra of the parent molecule, a) **DPTZ-DBT**, and the three substituted derivatives b) **DPTZ-*Me*-DBT**, c) **DPTZ-^{i}*Pr*-DBT**, and d) **DPTZ-^{t}*Bu*-DBT** in solvents of different polarity.

Table S1: S_0^{abs} is the energy (eV) of the ground state calculated relative to the other conformer, i.e. 0.0 is the lowest energy conformer for that molecule. The energy (eV) of the S_1 state at the Franck-Condon (Absorption, S_1^{abs}) and excited state optimised (Emission, S_1^{em}) geometries are also reported. The oscillator strengths are in brackets. Each structure was optimised in the absence of a solvent model to aid convergence. The final excited state emission energies were calculated using a SS-PCM approach using the solvent parameters of ethanol, anisole and toluene.

		toluene			anisole			ethanol		
		S_0^{abs}	S_1^{abs}	S_1^{em}	S_0^{abs}	S_1^{abs}	S_1^{em}	S_0^{abs}	S_1^{abs}	S_1^{em}
DPTZ–DBT	Axial	0.06	4.01	3.67 (0.043)	0.06	4.01	3.66 (0.044)	0.05	4.01	3.64 (0.044)
	Equatorial	0.00	3.88	2.78 (0.002)	0.00	3.91	2.53 (0.001)	0.00	3.94	2.19 (0.001)
DPTZ-*Me*-DBT	Axial	0.00	4.03	3.74 (0.041)	0.00	4.03	3.73 (0.042)	0.00	4.03	3.71 (0.043)
	Equatorial	1.09	-	2.81 (0.005)	1.08	-	2.60 (0.004)	1.08	-	2.31 (0.004)
DPTZ-^{i}*Pr*-DBT	Axial	0.00	4.04	3.74 (0.046)	0.00	4.04	3.73 (0.048)	0.00	4.05	3.71 (0.049)
	Equatorial	1.22	-	2.47 (0.003)	1.22	-	2.27 (0.003)	1.21	-	1.98 (0.002)
DPTZ-^{t}*Bu*-DBT	Axial	0.00	4.04	3.74 (0.046)	0.00	4.04	3.73 (0.048)	0.00	4.04	3.70 (0.049)
	Equatorial	1.06	-	2.51 (0.003)	1.05	-	2.50 (0.003)	1.05	-	2.48 (0.003)

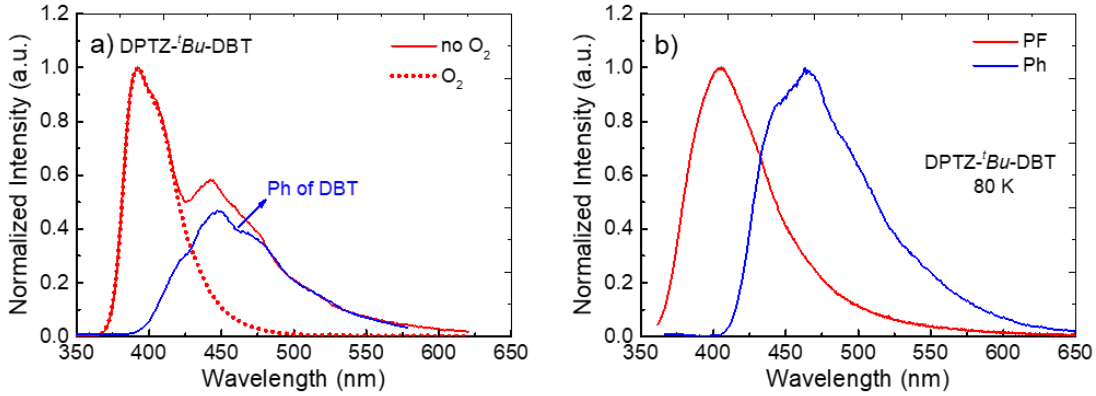

Figure S4- a) Steady-state emission spectra of **DPTZ-*^{t}Bu*-DBT** in zeonex at RT, obtained in aerated conditions and in vacuum. The phosphorescence of the DBT unit is also shown matching the phosphorescence of **DPTZ-*^{t}Bu*-DBT**. b) Time resolved fluorescence and phosphorescence spectra of **DPTZ-*^{t}Bu*-DBT** obtained at 80 K, collected at 1.1 ns and 50.1 ms, respectively.

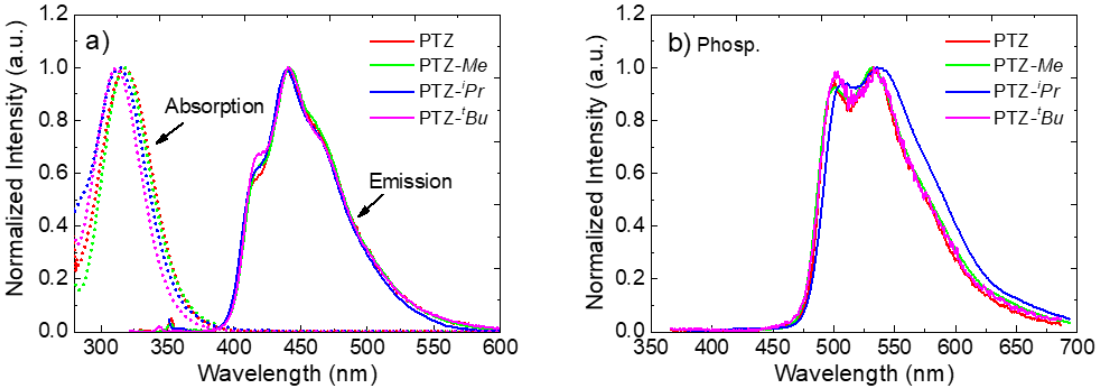

Figure S5. a) Comparison of the absorption (dot lines) and emission (full lines) spectra of PTZ and substituted PTZ units, PTZ-*Me*; PTZ-*^{i}Pr*; and PTZ-*^{t}Bu*. Absorption spectra were measured in toluene solution, and fluorescence in zeonex at RT. b) Phosphorescence of PTZ derivatives in zeonex film at 80 K.

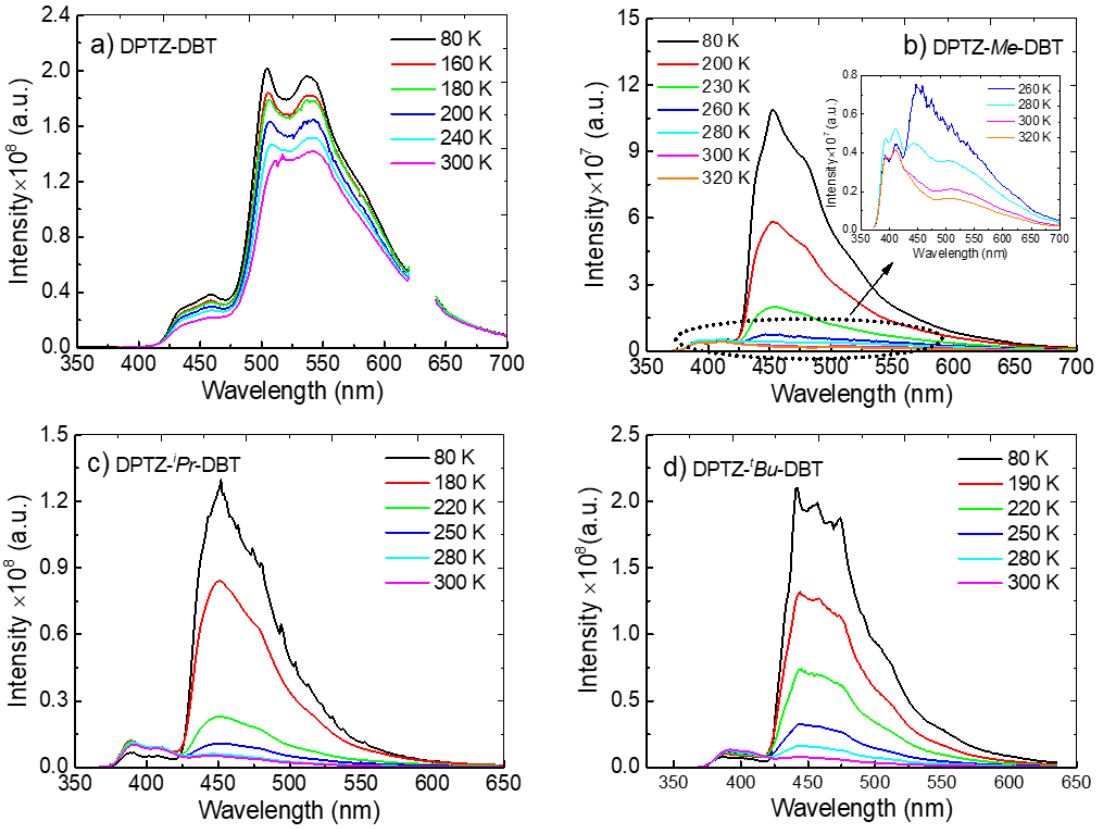

Figure S6- Steady-state emission spectra in zeonex, collected as a function of temperature. a) **DPTZ-DBT**, b) **DPTZ-*Me*-DBT**, c) **DPTZ-^{i}*Pr*-DBT**, d) **DPTZ-^{t}*Bu*-DBT**.

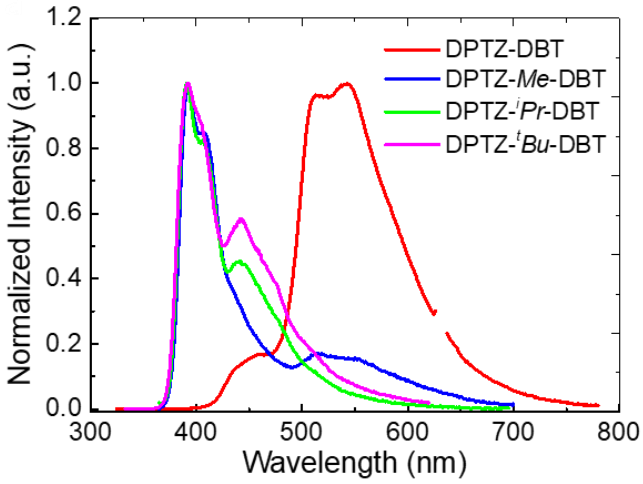

Figure S7-Comparison of the emission spectra of the four compounds in zeonex film in the absence of oxygen at RT. The second order of the Rayleigh scatter peak was removed around 650 nm.

S5 – Computational data

Computational Details. The ground and excited state geometries of all structures were optimized using (time-dependent) density functional theory within the approximation of the M062X exchange and correlation functional[4] as implemented within the Gaussian Quantum Chemistry package.[5] A Def2-SVP basis set was used throughout. To aid convergence, the effect of the solvent was not included during the geometry optimizations. However, all excited state energies included the solvent effect using a polarizable continuum model and the dielectric constant of toluene, anisole or ethanol. Fluorescence and phosphorescence energies were calculated using the S_1 and T_1 optimized geometries and a state-specific polarizable continuum model (SS-PCM).[6] Following recent work,[7] both the H-intra and H-extra folded conformers of the phenothiazine that allow formation of parallel quasi-axial (ax) and perpendicular quasi-equatorial (eq) conformers were investigated. However, in both cases one dominant conformer was found for both **DPTZ-DBT** and **DPTZ-*t*Bu-DBT**. For the former, both donor groups are equatorial to the acceptor, while in **DPTZ-*t*Bu-DBT** both donor groups are axial to the acceptor. The spin-orbit coupling calculations were performed using the Q-chem quantum chemistry software.[8]

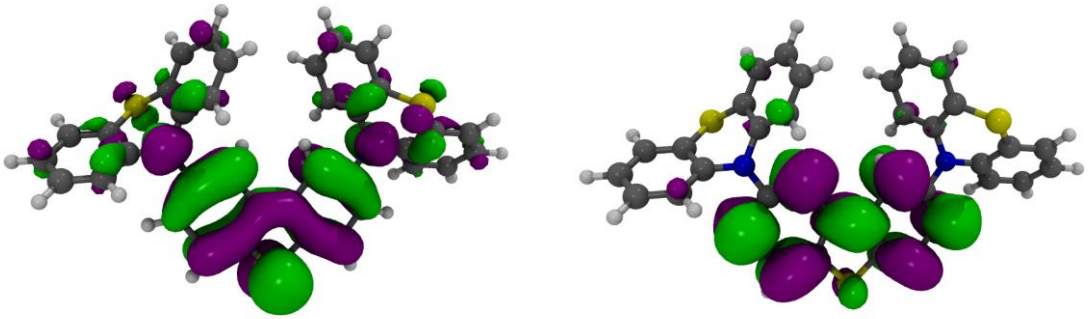

Figure S8 – The HOMO and LUMO orbitals of the axial form of **DPTZ-DBT**

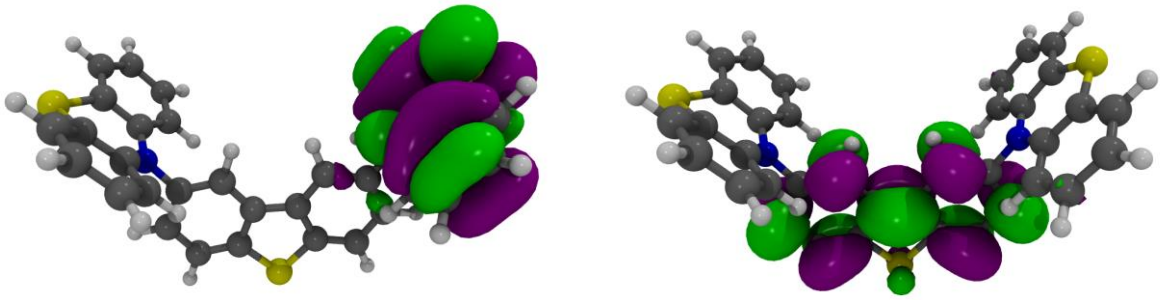

Figure S9 – The HOMO and LUMO orbitals of the equatorial form of **DPTZ-DBT**

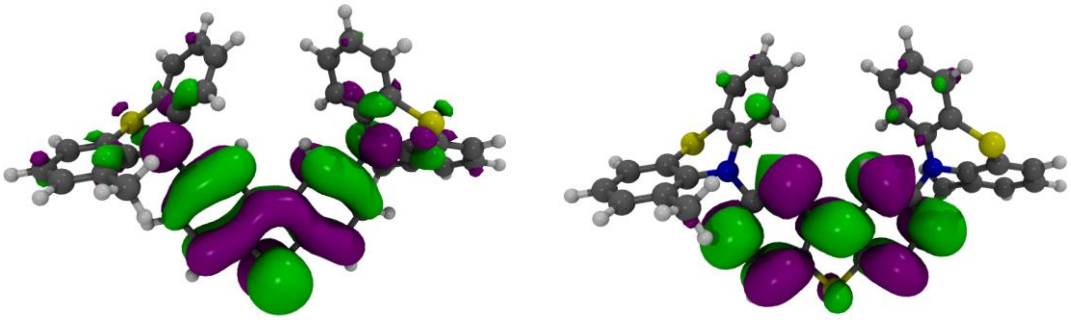

Figure S10 – The HOMO and LUMO orbitals of the axial form of **DPTZ-*Me*-DBT**

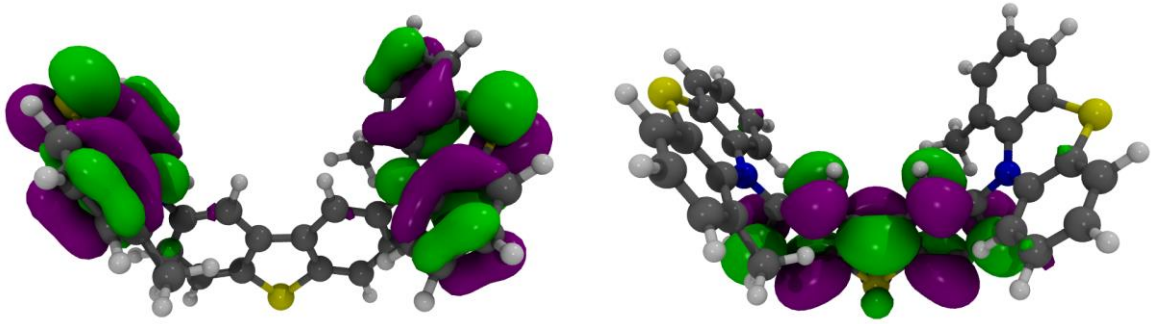

Figure S11 – The HOMO and LUMO orbitals of the equatorial form of **DPTZ-*Me*-DBT**

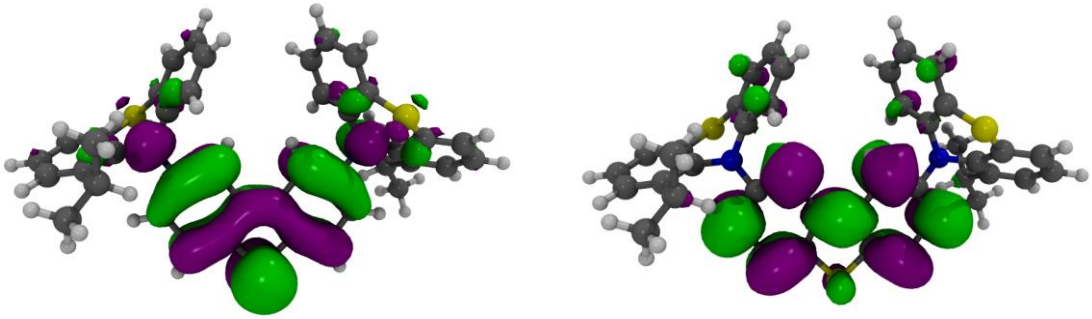

Figure S12 – The HOMO and LUMO orbitals of the axial form of **DPTZ-^{i}*Pr*-DBT**

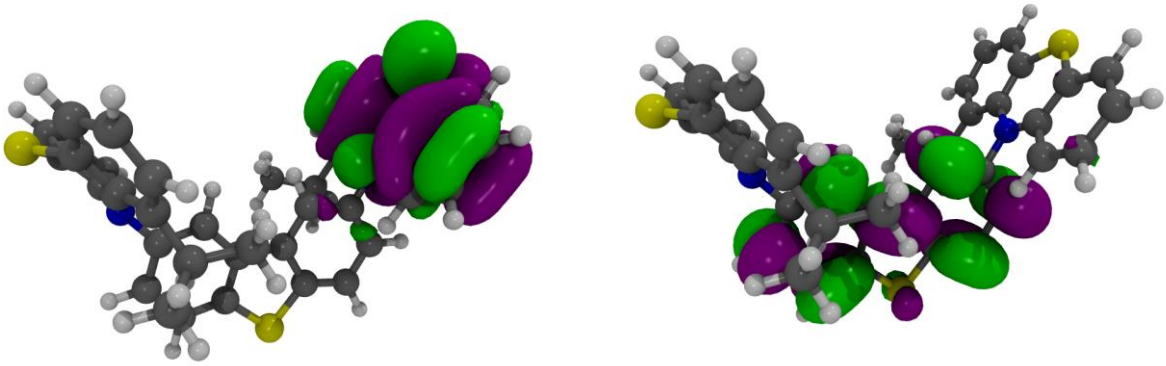

Figure S13 – The HOMO and LUMO orbitals of the equatorial form of **DPTZ-^{i}*Pr*-DBT**

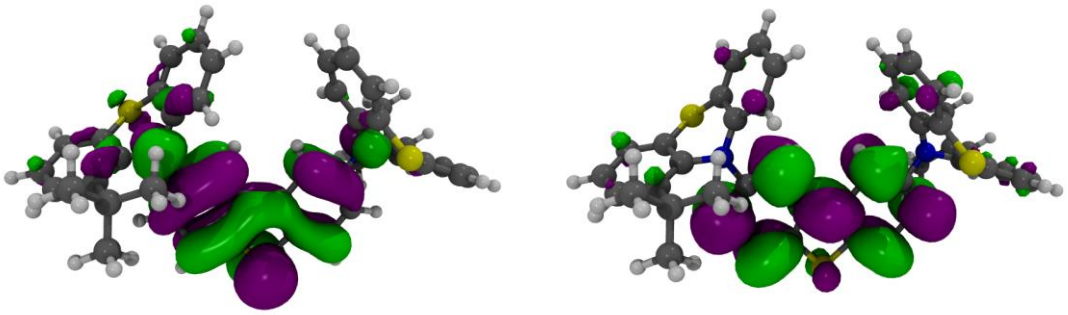

Figure S14 – The HOMO and LUMO orbitals of the axial form of **DPTZ-*^{t}Bu*-DBT**

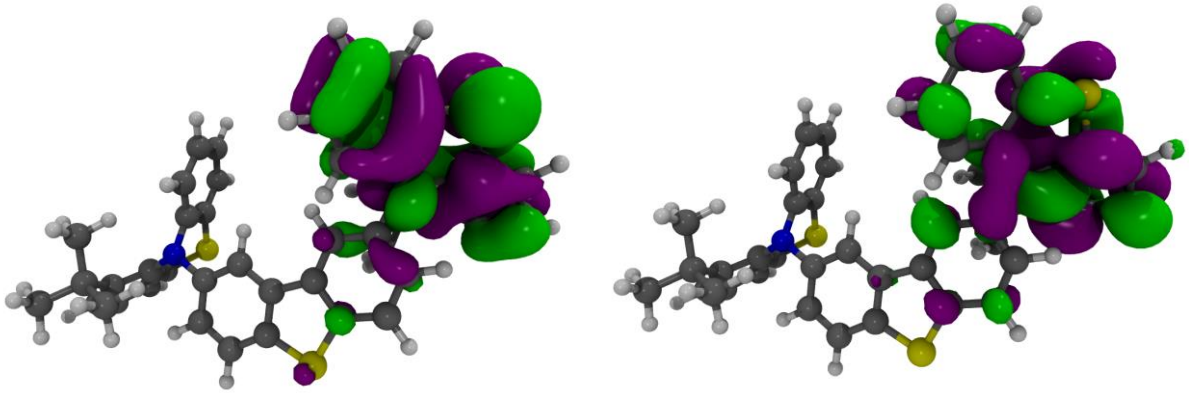

Figure S15 – The HOMO and LUMO orbitals of the equatorial form of **DPTZ-*^{t}Bu*-DBT**

S6- X-Ray Crystallography

X-Ray Crystallography. X-ray diffraction experiments were carried out on a Bruker 3-circle D8 Venture diffractometer with a PHOTON 100 CMOS area detector, using Mo-K_α or Cu-K_α radiation from IμS microsources with focussing mirrors. Crystals were cooled to 120 K using a Cryostream 700 (Oxford Cryosystems) open-flow N_2 gas cryostat. Absorption corrections were performed with SADABS 2014/5 or 2016/2 programs,[9] based on Laue equivalents and multiple scans, or (for **DPTZ-*^{i}*Pr-DBT**) by Gaussian integration based on crystal face indexing. The structures were solved by direct methods using SHELXS 2013/1 software,[10] or (for **DPTZ-*^{i}*Pr-DBT**) by intrinsic phasing method using SHELXT software[11] and refined by full-matrix least squares using SHELXL 2016/6 software[12] on OLEX2[13] platform. **DPTZ-Me-DBT**·$CHCl_3$ crystallised as non-merohedral twin of two components (in a 0.674(1):0.326(1) ratio) related by a 180° rotation around the reciprocal axis [0 1 0]*; the data were deconvoluted using CELL_NOW 2008/4 program and scaled with TWINABS 2012/1 program.[14] Crystal data and experimental details are listed in Table S1. Full crystallographic data have been deposited with Cambridge Structural Database, CCDC-1846156 to 1846161.

Relevant conformational parameters obtained from the X-ray crystallographic data for **DPTZ–DBT**, **DPTZ–*Me*–DBT** and **DPTZ–*^{i}Pr*–DBT** are listed in Table S2. The DBT moiety is practically planar or shows a slight twist, quantified by the angle ω between its two arene rings. The PTZ moiety

is always folded along the N…S vector, the folding angle θ (between its arene 'wings') varying substantially (*vide infra*). As discussed elsewhere,[7] mutual orientations of the PTZ and DBT moieties in crystals follow two main options, viz. the equatorial conformation whereby the PTZ moiety lies astride the DBT plane and is roughly perpendicular to it, and the axial conformation, where the PTZ is tilted to one side of the DBT plane. In the axial conformation, the torsion angle (τ) around the C(DBT)–N(PTZ) bond, measured between the p_π(C) orbital and the N lone pair, is close to zero; in the equatorial conformation, $\tau \approx 90°$. With two PTZ substituents present, their axial conformations can be either *cis* or *trans* with respect to the DBT plane, and there is an additional degree of flexibility (within both axial and equatorial options) as each PTZ moiety can fold in two opposite directions. The axial conformation allows the lone pair of the N atom to be conjugated with the π-system of the DBT, while the equatorial conformation precludes this, thereby favouring the competing conjugation with the arene rings of PTZ itself, as indicated by the N-C bond lengths (Table S3).

Slow evaporation of a **DPTZ–DBT** solution in $CDCl_3$, yielded concomitantly two crystalline phases, **DPTZ–DBT**·$CDCl_3$ and **DPTZ–DBT**·½$CDCl_3$. In both structures, the asymmetric unit contains one host molecule with both PTZ groups adopting equatorial orientations, the cavity between these groups filled by a disordered $CDCl_3$ molecule of crystallisation (Fig. S16). In the monosolvate, both PTZ moieties are folded outwards, while in the hemisolvate, one is folded outward and the other inward; the latter has a narrower θ angle (145°) that the rest (155-157°).

Crystallisation of **DPTZ–Me–DBT** from chloroform/hexane solution yielded in succession three crystalline phases, viz. chloroform monosolvate, solvent-free monoclinic and solvent-free triclinic. The asymmetric unit of **DPTZ–Me–DBT**·$CDCl_3$ comprises two host molecules (and two chloroform molecules), both adopting a *trans*-axial-conformation (Fig. S17a). In one molecule, the methyl substituents at both PTZ moieties are disordered, i.e. different conformers share the site, while the other molecule shows no disorder. The monoclinic unsolvated phase (Fig. S17b) has one independent molecule, which adopts a *cis*-axial-conformation. One whole PTZ-Me moiety is disordered between two orientations with methyl substituent on opposite sides, with occupancies refined to 0.769(3) and 0.231(3). The moiety is pivoted around N(1) so as to maximise the steric overlap between two conformers. The other PTZ moiety is ordered but its methyl substituent is distributed between two positions in a 0.7:0.3 ratio. The triclinic phase also has one independent molecule with one PTZ moiety ordered and the other disordered in a 2:1 ratio, but in contrast to the monoclinic polymorph, the overall conformation is *trans*-axial (Fig. S17c). Curiously, the minor PTZ conformation has the methyl substituent further disordered (occupancies 0.25 and 0.08). The molecule of **DPTZ–^{i}Pr–DBT** has crystallographic C_2 symmetry and thus a *trans*-axial-conformation (Fig. S18), showing no disorder.

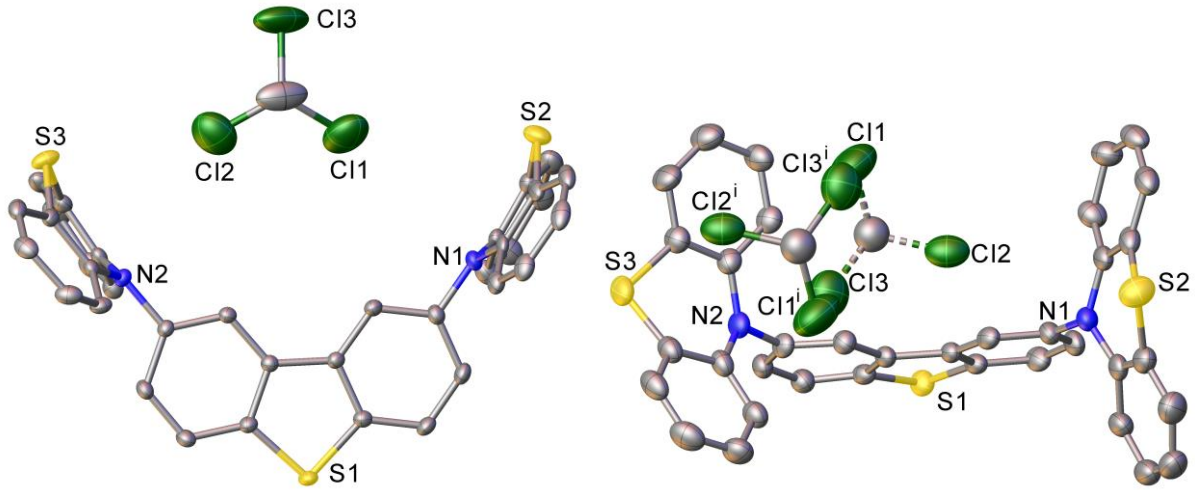

Figure S16. X-ray molecular structures of **DPTZ–DBT**·$CDCl_3$ (a) and **DPTZ–DBT**·½$CDCl_3$ (b). Thermal ellipsoids are drawn at the 50% probability level, H atoms are omitted for clarity. The $CDCl_3$ molecule is (a) disordered in a general position (minor orientation is omitted), or (b) disordered between two half-occupied inversion-related positions.

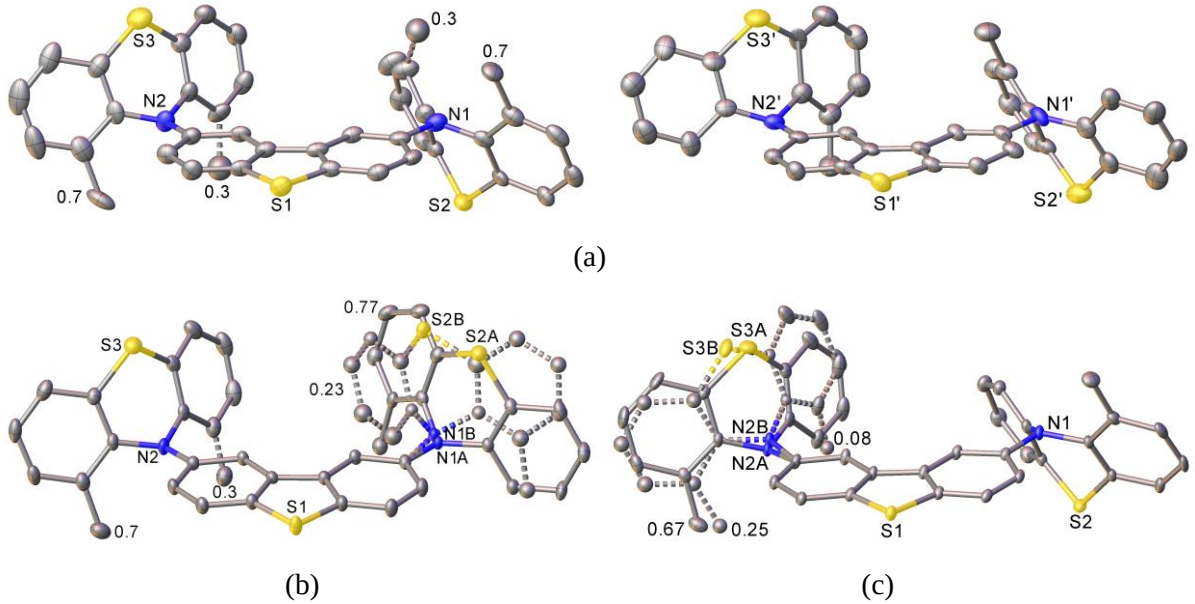

Figure S17. DPTZ–Me–DBT molecules in the crystal of its $CHCl_3$ solvate (a), monoclinic (b) and triclinic (c) polymorphs. Thermal ellipsoids are drawn at the 30% probability level, H atoms are omitted. Occupancies of the disordered groups/atoms are cited. The numbers on figures (b) and (c) are the fraction percent occupancies at disordered sites.

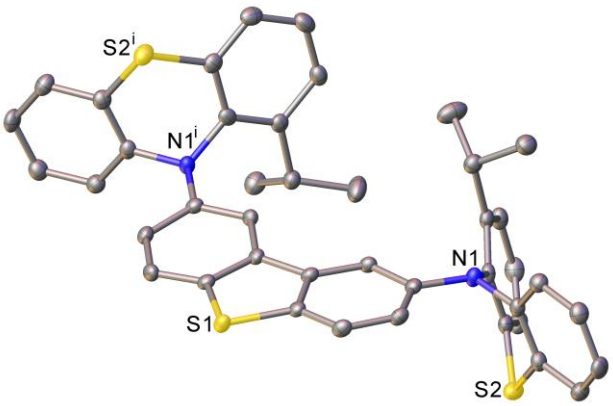

Figure S18. X-ray molecular structure of **DPTZ–^{i}Pr–DBT**. Thermal ellipsoids are drawn at the 50% probability level, H atoms are omitted. Primed atoms are generated by the twofold axis.

Table S2. Crystal data

Compound	**DPTZ-DBT** ·$CDCl_3$	**DPTZ-DBT**·½$CDCl_3$	**DPTZ-Me-DBT**·$CHCl_3$	**DPTZ-Me-DBT**	**DPTZ-Me-DBT**	**DPTZ-*i*Pr-DBT**
Depository code	17srv182	17srv187	17srv241	17srv251	17srv254	17srv247
CCDC no.	1846156	1846157	1846158	1846159	1846160	1846161
Formula	$C_{37}H_{23}Cl_3DN_2S_3$	$C_{36.5}H_{22}D_{0.5}Cl_{1.5}N_2S_3$	$C_{39}H_{27}Cl_3N_2S_3$	$C_{38}H_{26}N_2S_3$	$C_{38}H_{26}N_2S_3$	$C_{42}H_{34}N_2S_3$
$D_{calc.}$/ g cm^{-3}	1.426	1.450	1.404	1.345	1.337	1.374
μ/mm^{-1}	0.505	3.815	4.367	2.496	0.277	2.379
Formula Weight	699.11	638.92	726.15	606.79	606.79	662.89
T/K	120	120	120	120	120	120
Crystal System	triclinic	triclinic	triclinic	monoclinic	triclinic	monoclinic
Space Group	$P\bar{1}$ (no. 2)	$P\bar{1}$ (no. 2)	$P\bar{1}$ (no. 2)	$P2_1/n$ (no. 14)	$P\bar{1}$ (no. 2)	$C2/c$ (no. 15)
a/Å	7.2606(4)	8.6239(3)	11.0581(4)	11.7234(4)	7.9477(4)	27.5841(7)
b/Å	13.8198(7)	13.7187(5)	15.5487(6)	14.3733(4)	11.9549(7)	14.4337(4)
c/Å	17.5138(9)	14.3075(6)	20.2305(8)	18.1421(6)	15.9521(9)	8.0484(2)
α/°	105.2745(17)	66.090(2)	93.782(2)	90	91.458(2)	90
β/°	94.047(2)	74.501(3)	97.083(2)	101.501(2)	95.161(2)	90.3137(14)
γ/°	103.967(2)	73.864(3)	93.686(2)	90	92.542(2)	90
V/Å^3	1628.15(15)	1463.27(10)	3435.1(2)	2995.63(17)	1507.38(14)	3204.35(14)
Z	2	2	4	4	2	4
λ/Å	0.71073	1.54184	1.54184	1.54184	0.71073	1.54184
Radiation type	MoK_α	CuK_α	CuK_α	CuK_α	MoK_α	CuK_α
Θ_{max}/°	27.5	66.6	59.0	66.6	30.0	74.2

Reflections total	22741	17147	34432	25201	32928	10536
unique	7464	4996	21960	5016	8786	2995
with $I > 2\sigma(I)$	5670	3101	13875	3425	6612	2408
R_{int}	0.050	0.079	0.057	0.084	0.035	0.038
Parameters/restraints	422, 3	405, 15	894, 825	451, 62	451, 538	218, 0
Δρ, max/min, eÅ^{-3}	0.73, -0.66	0.47, -0.55	0.76, -0.59	0.46, -0.35	0.44, -0.40	0.34, -0.25
Goodness of fit	1.021	1.034	1.025	1.077	1.032	1.009
R_1 , wR_2 (all data)	0.077, 0.143	0.115, 0.166	0.138 , 0.193	0.096 , 0.113	0.070 , 0.118	0.050 , 0.086
R_1, wR_2 [$I > 2\sigma(I)$]	0.054 , 0.131	0.059 , 0.136	0.079 , 0.165	0.056 , 0.102	0.047 , 0.109	0.035 , 0.080

Table S3. Selected dihedral angles (°)

	θ_1[a]	τ_1[b]	θ_2[a]	τ_2[b]	ω[c]
DPTZ-DBT·$CDCl_3$	155.3(1)	84.7(2)	155.0(1)	76.1(2)	1.8(1)
DPTZ-DBT·½$CDCl_3$	157.0(2)	87.6(2)	145.2(2)	83.7(3)	7.6(1)
DPTZ-Me-DBT·$CHCl_3$[d]	134.3(3)	2.3(5)	135.3(3)	1.3(5)	0.4(3)
	135.2(3)	1.2(4)	137.9(3)	8.8(5)	1.5(3)
DPTZ-Me-DBT, monocl.	140.0(2)	10.5(4)	132.5(1)	0.2(2)	2.7(1)
	143.9(1)[e]	18.3(1)[e]			
DPTZ-Me-DBT, tricl.	137.0(1)	4.7(1)	134.9(1)	6.4(1)	2.4(1)
			134.8(2)[d]	20.4(8)[d]	
DPTZ-^{i}Pr-DBT	133.2(1)	11.9(1)	---	---	9.2(1)

[a] The PTZ moiety is always folded along the N…S vector; θ is the folding angle between its arene 'wings'. [b] τ is the torsion angle around the C(DBT)–N(PTZ) bond, measured between the p_π(C) orbital and the N lone pair. [c] ω is the angle between the two outer arene of the near-planar DBT moiety. [d] Two independent molecules. [e] Minor position of the disordered moiety.

[1] J.S. Ward, R. S. Nobuyasu, A. S. Batsanov, P. Data, A. P. Monkman, F. B. Dias and M. R. Bryce, *Chem. Commun.*, 2016, **52**,2612-2615.

[2] R. Huang, J. Avó, T. Northey, E. Chaning-Pearce, P. L. dos Santos, J. S. Ward, P. Data, M. K. Etherington, M. A. Fox, T. J. Penfold, M. N. Berberan-Santos, J. C. Lima, M. R. Bryce and F. B. Dias, *J. Mater. Chem. C*, 2017, **5**, 6269–6280.

[3] A. A. Lamola and G. S. Hammond, *J. Chem. Phys.,* 1965, **43**, 2129-2135

[4] Y Zhao and D G Truhlar, *Theor. Chem. Acc*. 1999 **120**,215-241

[5] M. J. Frisch et. al. Gaussian 09 Revision A.1, Gaussian Inc., Wallingford CT, 2009

[6] W. Gyorffy, T. M. Henderson, J. C. Greer *J. Chem. Phys*., 2006, 125, 054104.

[7] M. K. Etherington, F. Franchello, J. Gibson, T. Northey, J. Santos, J. S. Ward, H. F. Higginbotham, P. Data, A. Kurowska, P. L. Dos Santos, D. R. Graves, A. S. Batsanov, F. B. Dias, M. R. Bryce, T. J. Penfold and A. P. Monkman, *Nat. Commun.*, 2017, **8**, 14987.

[8] Y. Shao et al., Mol. Phys., 2015, **113,** 184-215.

[9] L. Krause, R. Herbst-Irmer, G. M. Sheldrick and D. Stalke, *J. Appl. Crystallogr*., 2015, **48**, 3–10.

[10] G. M. Sheldrick, *Acta Crystallogr. Sect. A*, 2008, **64**, 112–122.

[11] G. M. Sheldrick, *Acta Crystallogr. Sect. A*, 2015, **71**, 3–8.

[12] G. M. Sheldrick, *Acta Crystallogr. Sect. C*, 2015, **71**, 3–8.

[13] O. V. Dolomanov, L. J. Bourhis, R. J. Gildea, J. A. K. Howard and H. Puschmann, *J. Appl. Crystallogr*., 2009, **42**, 339–341.

[14] G. M. Sheldrick, *TWINABS.* Version 2012/1. Georg-August-Universität Göttingen, Göttingen, Germany, 2012.